

Supporting Information

for

Hydrophilic Mesoporous Poly(ionic liquid) Supported Au-Pd Alloy Nanoparticles towards Aerobic Oxidation of 5-hydroxymethylfurfural to 2, 5-furandicarboxylic acid under Mild Condition

Qian Wang, Wei Hou, Shuai Li, Jingyan Xie, Jing, Li, Yu Zhou, Jun Wang**

State Key Laboratory of Materials-Oriented Chemical Engineering, College of Chemical Engineering, Nanjing Tech University (formerly Nanjing University of Technology), Nanjing, 210009, China

*Corresponding author, Tel: +86-25-83172264, Fax: +86-25-83172261

E-mail: njutzhouyu@njtech.edu.cn (Y. Zhou); junwang@njtech.edu.cn (J. Wang).

Supplementary Materials

1. Supplementary Experimental	S2
2. Supplementary Scheme	S3
3. Supplementary Figures	S5
4. Supplementary Tables	S13
5. References	S15

1. Supplementary Experimental

Synthesis of Au₁-Pd₁@PECN(PVP)

PECN (0.50 g) was mixed with 20 mL aqueous solution containing ammonium tetrachloropalladate ((NH₄)₂PdCl₄, 13.4 mg, 1 wt%) and chloroauric acid (HAuCl₄·4H₂O, 10.45 mg, 1 wt%), and then stirred at room temperature for 24 h. After that, the solid was separated by centrifugation, washed with water, and then dried at 60 °C. The obtained pale yellow solid was emerged in a PVP solution (0.2 g in 20 mL water). The mixture was stirred at room temperature for 1 h and then the solid was separated by centrifugation, washed with deionized water, and then vacuum dried at 60 °C for 12 h. Reduction proceeded at 300 °C for 4 h under H₂ atmosphere, giving the product Au₁-Pd₁@PECN(PVP).

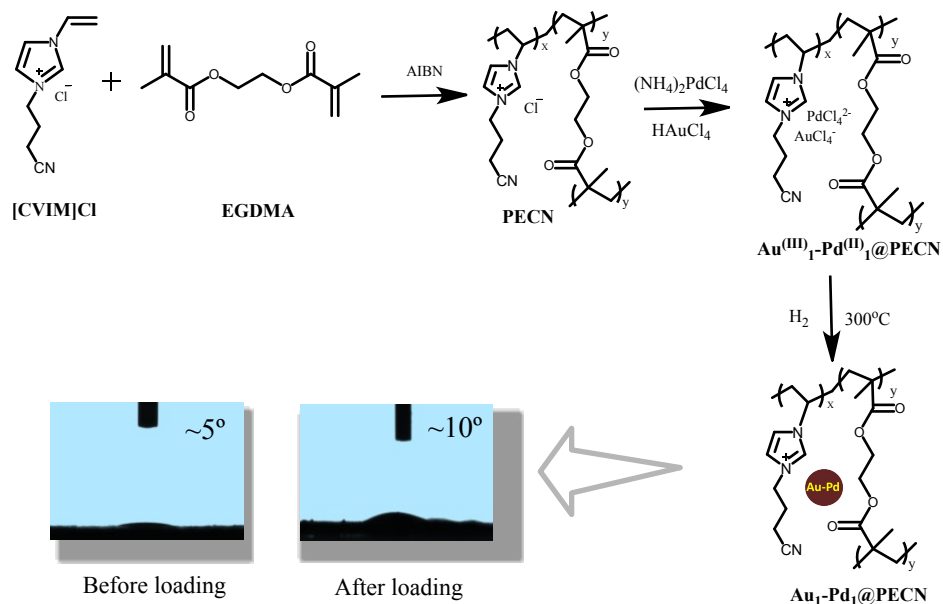
Synthesis of Au₁-Pd₁@PECN-S

PECN (0.50 g) was mixed with 20 mL aqueous solution containing ammonium tetrachloropalladate ((NH₄)₂PdCl₄, 13.4 mg, 1 wt%) and chloroauric acid (HAuCl₄·4H₂O, 10.45 mg, 1 wt%), and then stirred at room temperature for 24 h. After that, the solid was separated by centrifugation, washed with water, and then dried at 60 °C. Then the solid was dispersed in 20 mL water, followed with the dropwise addition of 0.015 g NaBH₄ aqueous solution 2 mL at 5 °C. The obtained precipitate was isolated by filtration and dried in vacuo at 60 °C for 12 h to give Au₁-Pd₁@PECN-S as a gray solid.

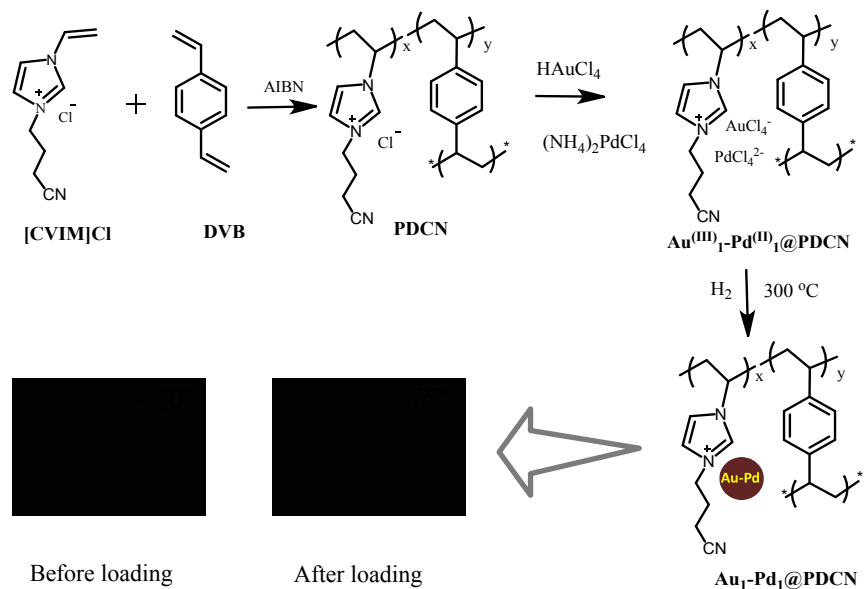
Synthesis of Au₁-Pd₁@PECN-S(PVP)

PECN (0.50 g) was mixed with 20 mL aqueous solution containing ammonium tetrachloropalladate ((NH₄)₂PdCl₄, 13.4 mg, 1 wt%) and chloroauric acid (HAuCl₄·4H₂O, 10.45 mg, 1 wt%), and then stirred at room temperature for 24 h. After that, the solid was separated by centrifugation, washed with deionized water, and then vacuum dried at 60 °C for 12 h. The solid was dispersed in 20 mL aqueous solution containing 0.2 g PVP, followed with the dropwise addition of 2 mL aqueous solution containing 0.015 g NaBH₄ at 5 °C. The obtained precipitate was isolated by filtration and dried at 60 °C to give Au₁-Pd₁@PECN-S(PVP) as a gray solid.

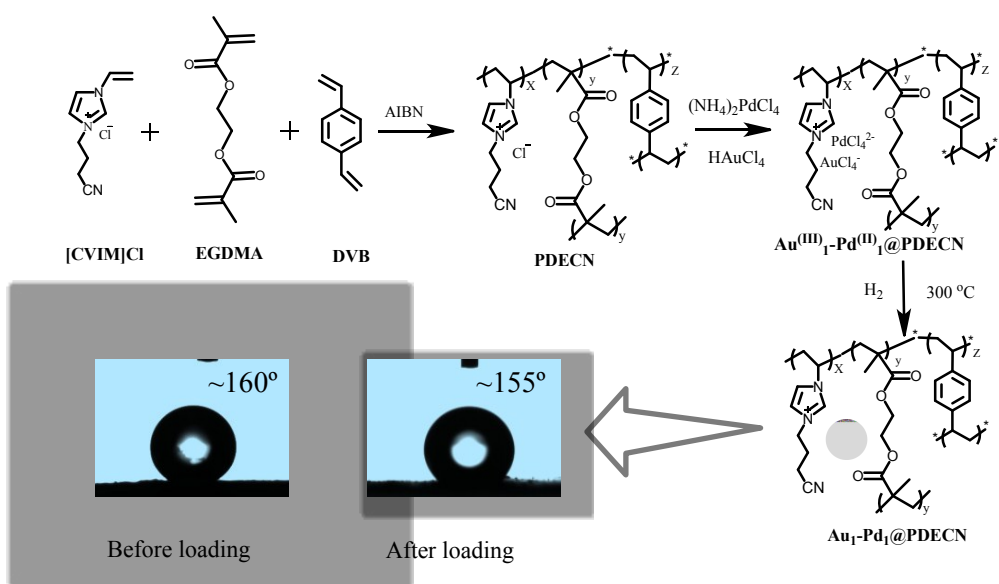
2. Supplementary Schemes



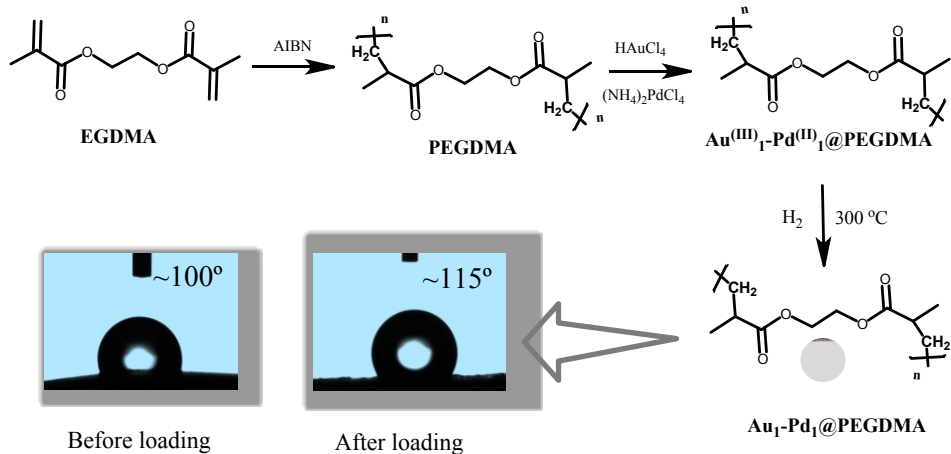
Scheme S1. Synthesis process of $\text{Au}_1\text{-Pd}_1@\text{PECN}$.



Scheme S2. Synthesis process of $\text{Au}_1\text{-Pd}_1@\text{PDCN}$.



Scheme S3. Synthesis process of $\text{Au}_1\text{-Pd}_1@\text{PDECN}$.



Scheme S4. Synthesis process of $\text{Au}_1\text{-Pd}_1@\text{PEGDMA}$.

3. Supplementary Figures

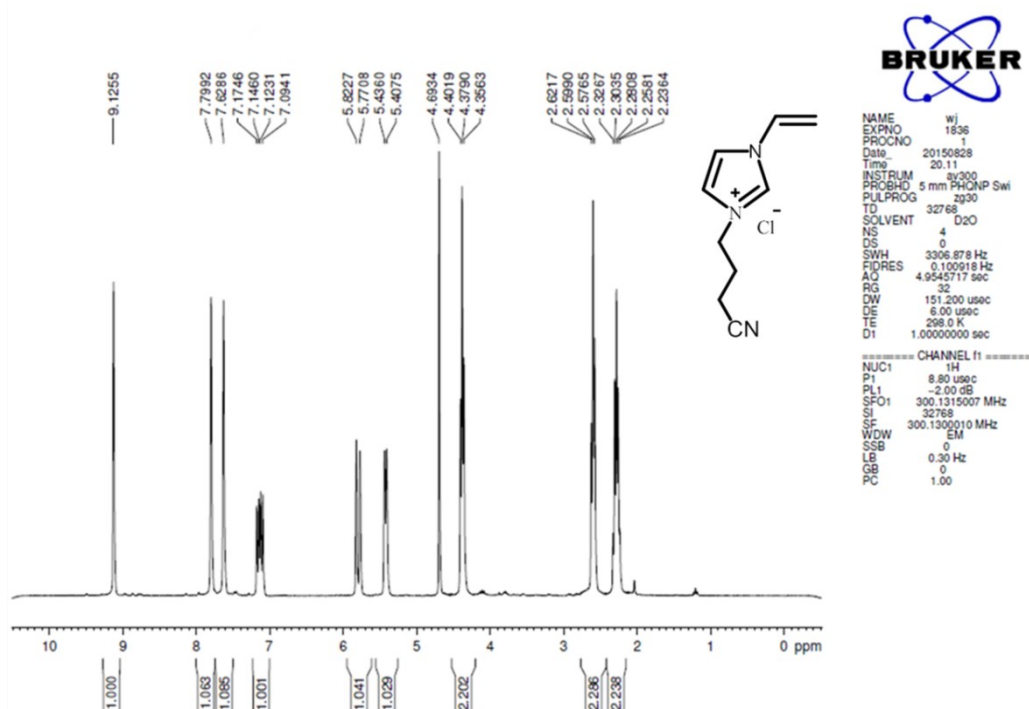


Fig. S1 ¹H-NMR spectrum of [CVIM]Cl. ¹H NMR (300 MHz, D₂O, TMS): δ (ppm) = 2.3 (q, 2H, -CH₂), 2.5 (t, 2H, -CH₂), 4.4 (t, 1H, -CH), 4.6 (t, 2H, -CH₂), 5.4 (d, 2H, -CH₂), 5.8 (d, 1H, -CH), 7.7 (d, 1H, -CH), 9.1 (s, 1H, -CH).

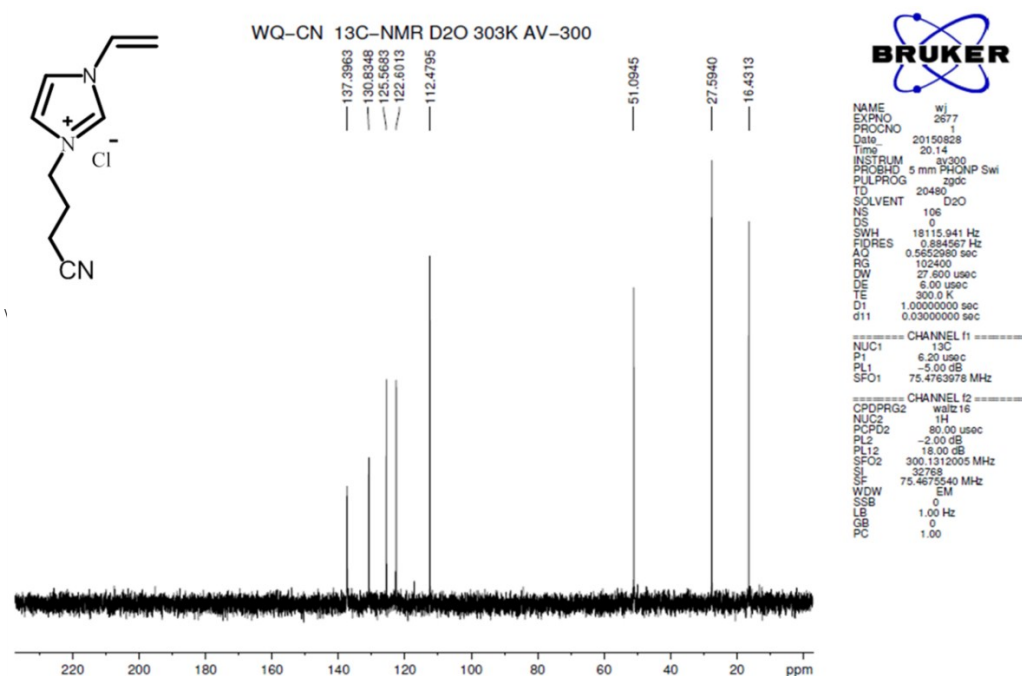


Fig. S2 ¹³C-NMR spectrum of [CVIM]Cl. ¹³C NMR (300 MHz, D₂O, TMS): δ 137.39, 130.83, 125.57, 122.60, 112.48, 51.09, 27.59, 16.43 ppm.

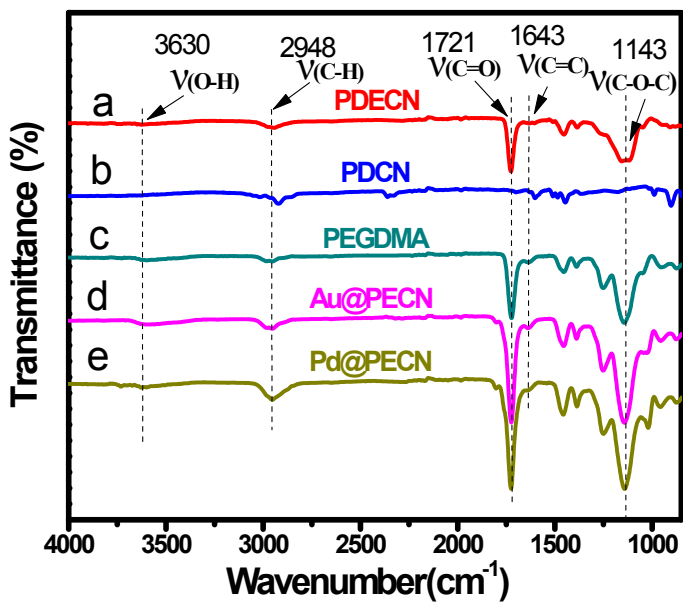


Fig. S3 FT-IR spectra of different samples.

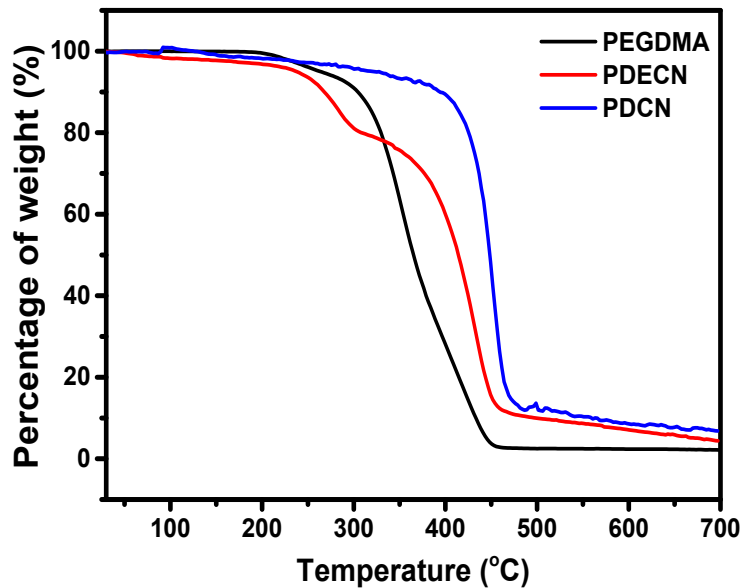


Fig. S4 TG curves of various supports.

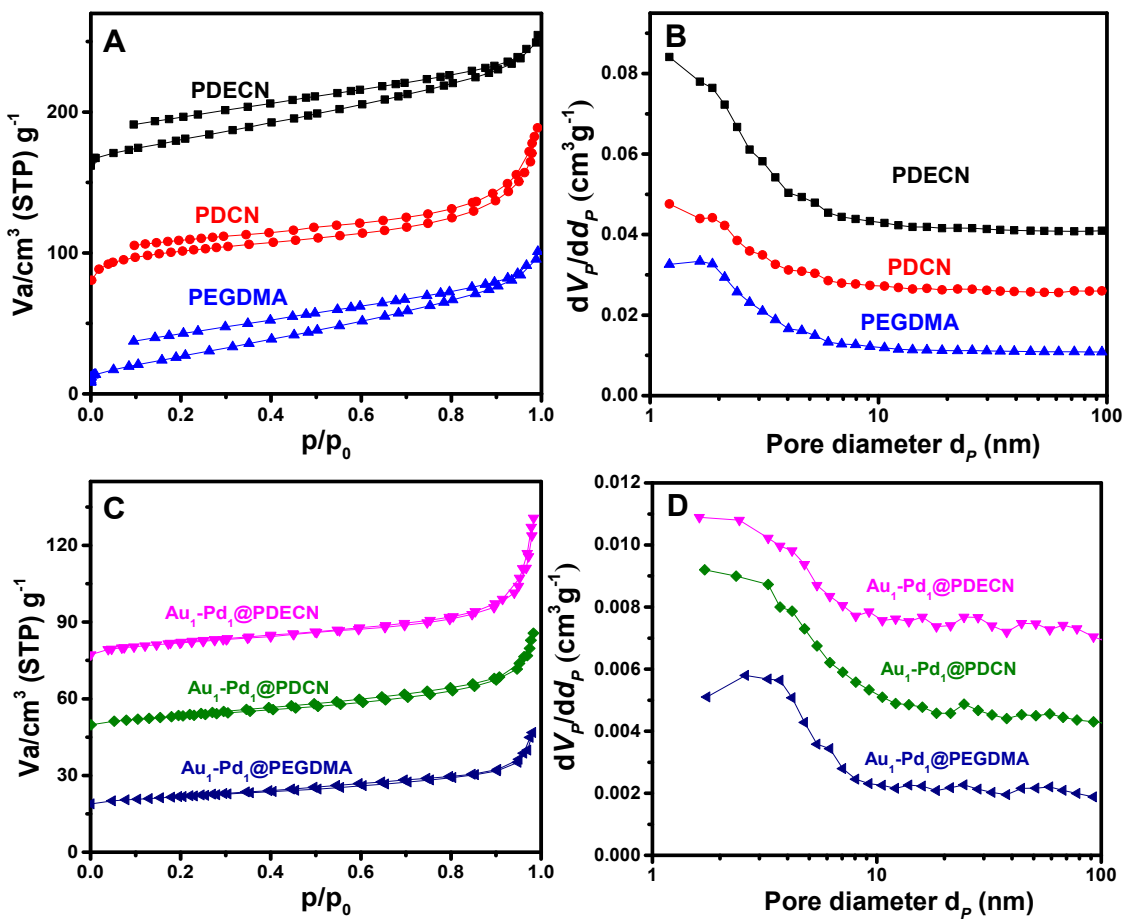


Fig. S5 (A) N₂ sorption isotherms and (B) pore size distribution curves of PDECN, PDCE, PEGDMA, (C) N₂ sorption isotherms and (D) pore size distribution curves of Au₁-Pd₁@PDECN, Au₁-Pd₁@PDCN, Au₁-Pd₁@PEGDMA.

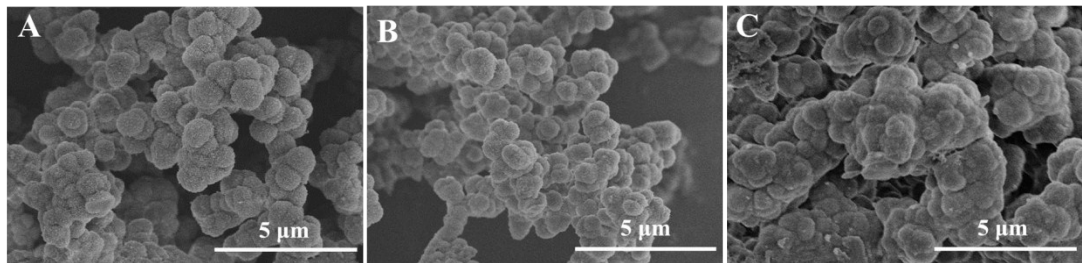


Fig. S6 SEM images of (A) PDECN, (B) PDCN and (C) PEGDMA.

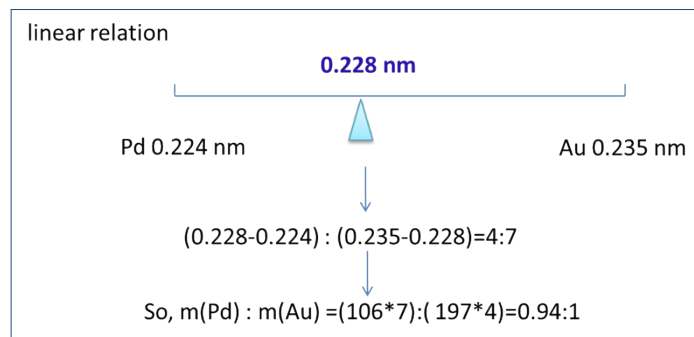


Fig. S7 Calculation of Au/Pd weight ratio in $\text{Au}_1\text{-Pd}_1@\text{PECN}$ according to the lattice spacing and their linear relationship.

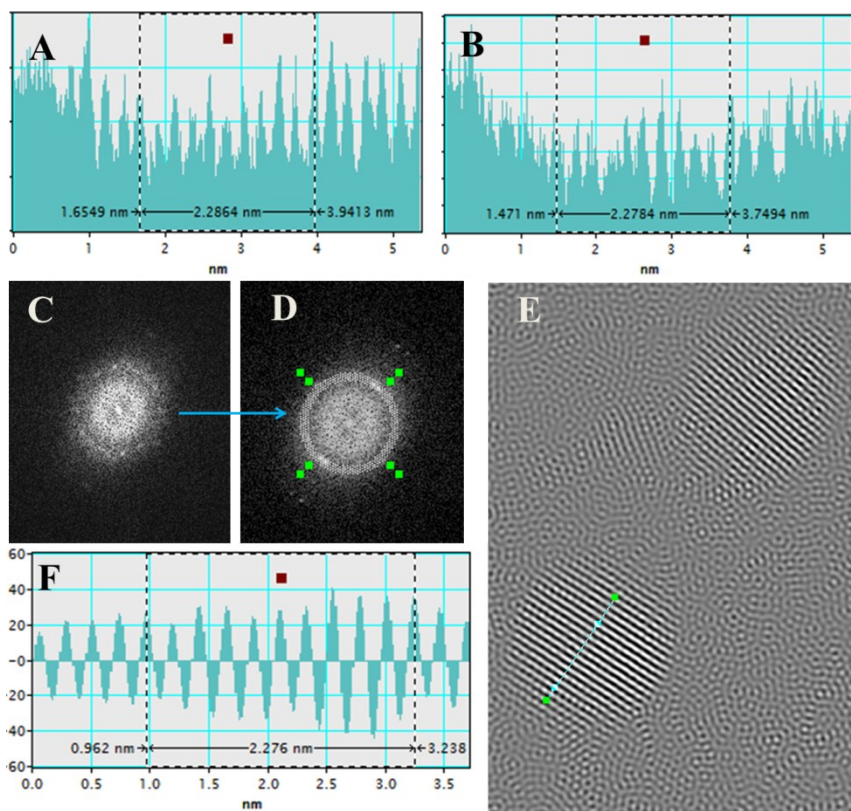


Fig. S8 Fringe spacing images tested by Fourier transform of (A) fresh and (B) recovered $\text{Au}_1\text{-Pd}_1@\text{PECN}$; (C, D) Electron diffraction patterns and (E, F) Fringe spacing images tested by inverse Fourier transform of $\text{Au}_1\text{-Pd}_1@\text{PECN}$.

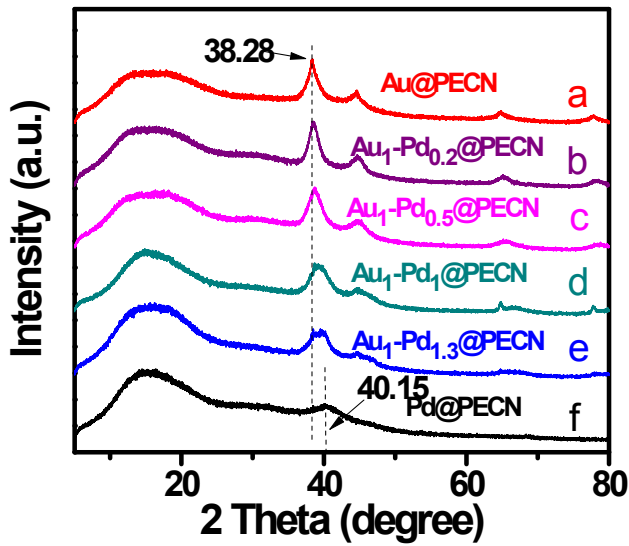


Fig. S9 XRD patterns of different samples. The reflections of metallic gold are detected at 38.28° and 44.3°, assignable to the (111) and (200) planes of fcc gold respectively. The broad peak at 12-22° is related to the amorphous carbon phase, while the peak related to Pd species is evidenced at 40.15°. As the Au/Pd ratio evolves from 1:0.2, 1:0.5, 1:1 to 1:1.3, there is a gradual peak shift to high angle, the characteristic peak of Pd@PECN at 40.15°.

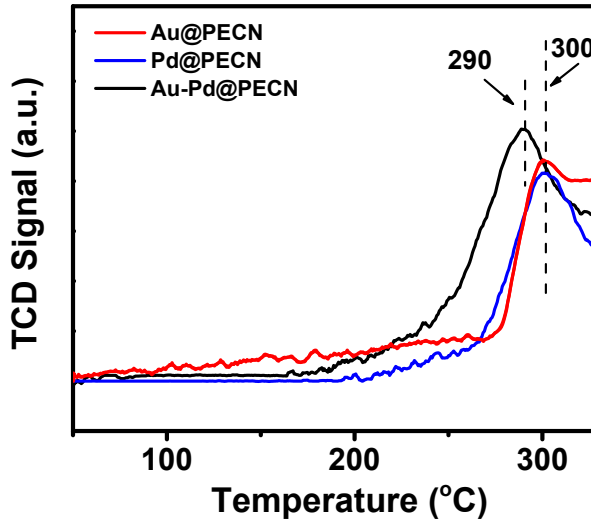


Fig. S10 TPR curves of Au@PECN, Pd@PECN and Au_{1-Pd₁@PECN}.

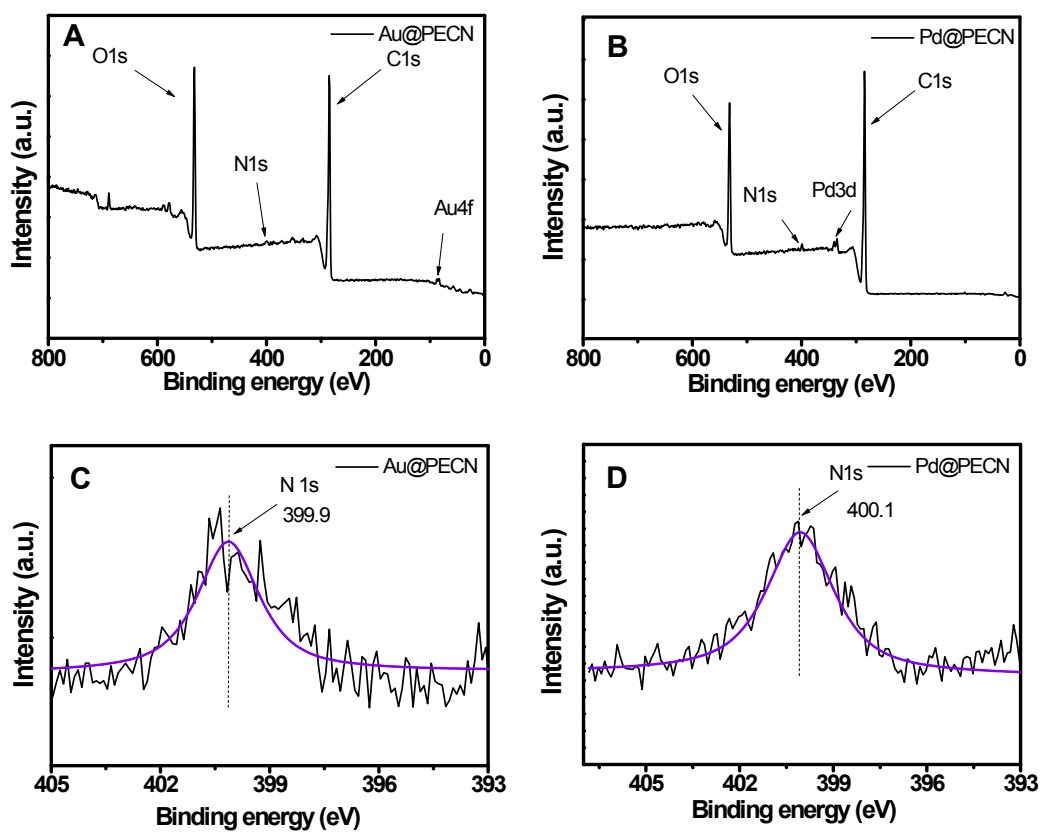


Fig. S11 XPS analysis for survey scan of (A) Au@PECN, (B) Pd@PECN; N1s spectra of (C)Au@PECN and (D) Pd@PECN.

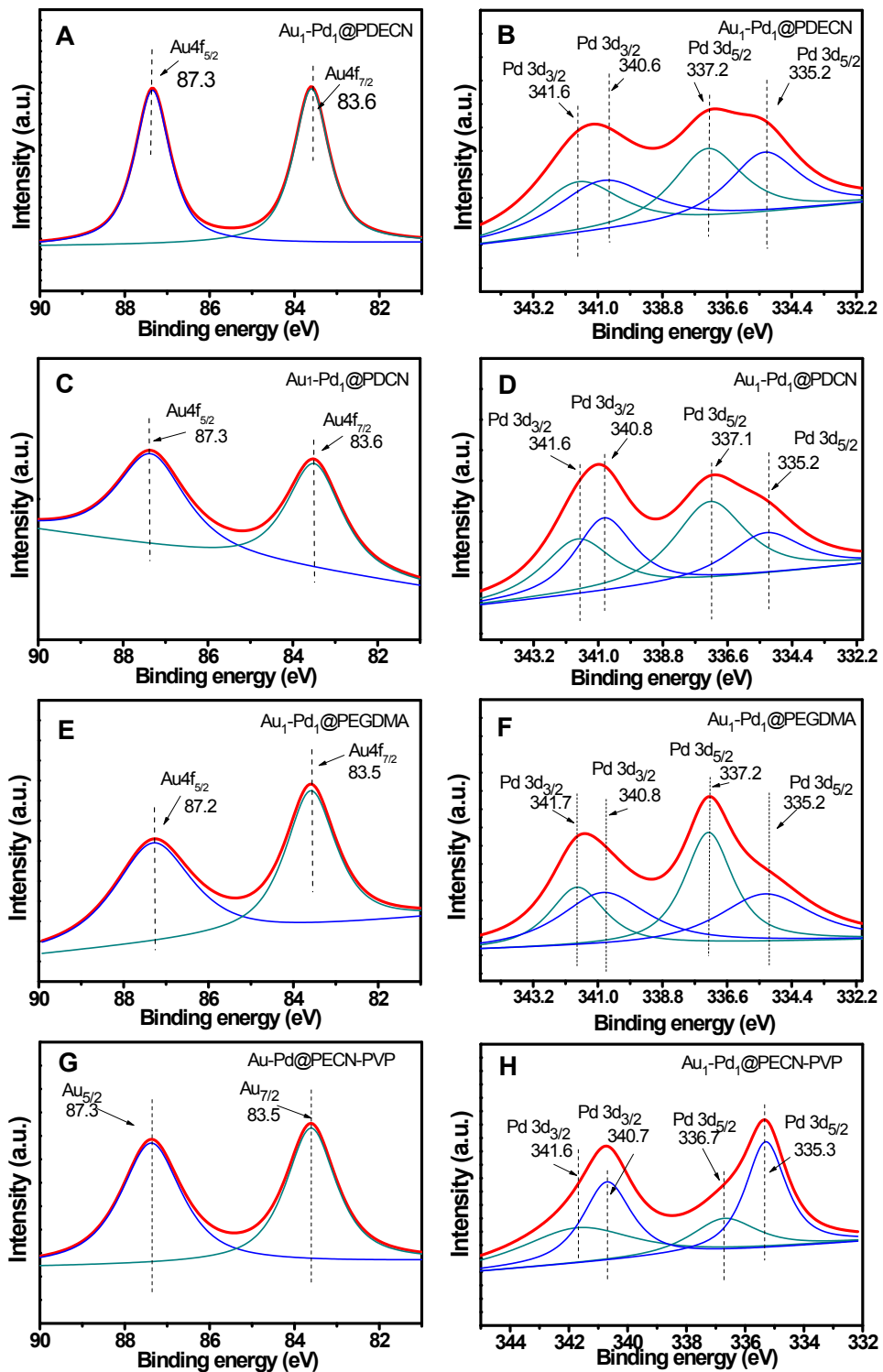


Fig. S12 Au 4f spectra of (A) Au₁-Pd₁@PDECN, (C) Au₁-Pd₁@PDCN, (E) Au₁-Pd₁@PEGDMA and (G) Au₁-Pd₁@PECN(PVP); Pd 3d XPS spectra of (B) Au₁-Pd₁@PDECN, (D) Au₁-Pd₁@PDCN, (F) Au₁-Pd₁@PEGDMA and (H) Au₁-Pd₁@PECN(PVP).

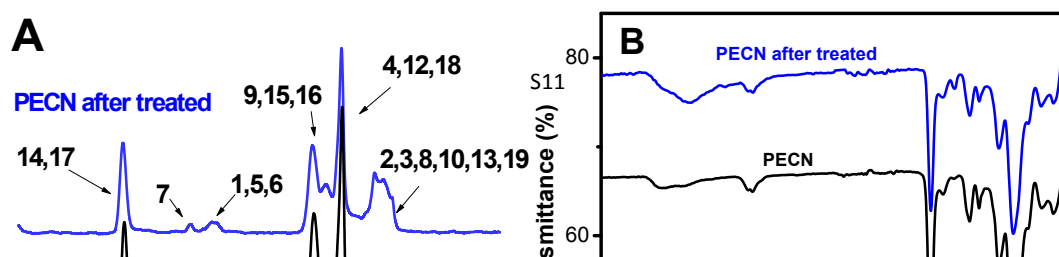


Fig. S13 (A) Solid ^{13}C -NMR and (B) FT-IR spectra of fresh and treated PECN. (PECN 0.02 g was mixed with 2 mL aqueous solution containing 0.4 mmol K_2CO_3 and stirred at 90 °C for 12 h, the simulation of reaction solution).

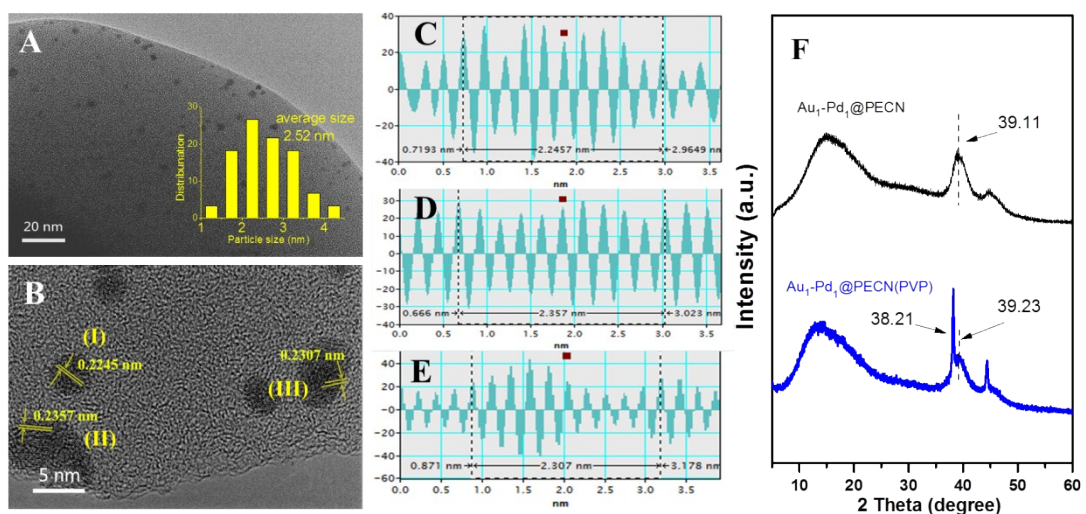


Fig. S14 (A, B) TEM images of $\text{Au}_1\text{-Pd}_1\text{@PECN(PVP)}$; Lattice fringe spacing of different nanoparticles in the area of (C) I, (D) II and (E) III in Figure B; (F) XRD patterns of $\text{Au}_1\text{-Pd}_1\text{@PECN}$ and $\text{Au}_1\text{-Pd}_1\text{@PECN(PVP)}$. Magnified TEM images reveal that $\text{Au}_1\text{-Pd}_1\text{@PECN(PVP)}$ contains Au NPs, Pd NPs and some alloy NPs with the mean size of 2.52 nm (Fig. S12B-E). XRD pattern of $\text{Au}_1\text{-Pd}_1\text{@PECN(PVP)}$ also shows obvious characteristic peak of Au and Pd NPs (Fig. S12F). These results suggest that PVP is resistive to form alloy although it is helpful to generate fine NPs.

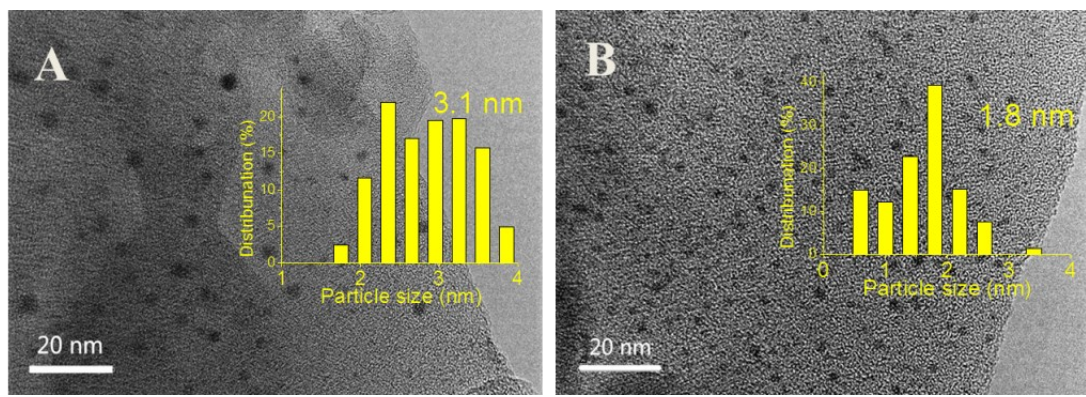


Fig. S15 TEM images of A) $\text{Au}_1\text{-Pd}_1@\text{PECN-S}$, B) $\text{Au}_1\text{-Pd}_1@\text{PECN-S(PVP)}$.

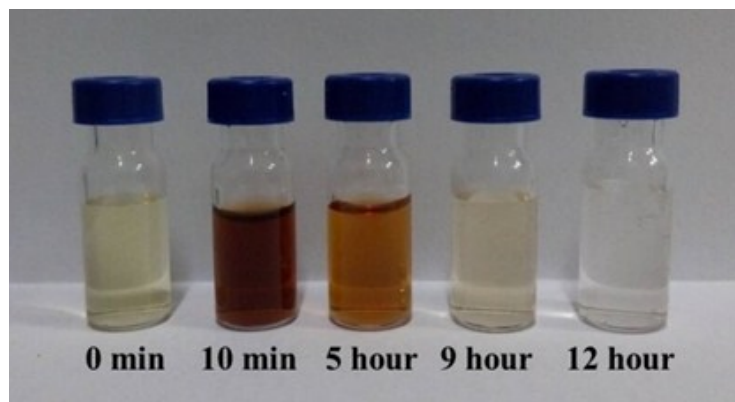


Fig. S16 Color change for the reaction mixtures at different times. Reaction conditions: HMF 0.1 mmol, HMF/metal molar ratio=100:1, O₂ 10 mL min⁻¹, K₂CO₃ 0.4 mmol, water 2 mL, 90 °C.

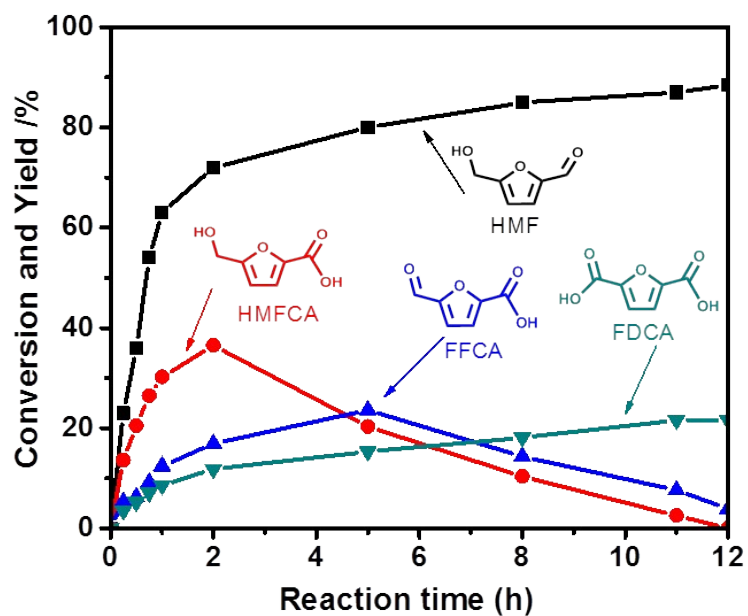


Fig. S17 Time-resolved conversion and yield in Au₁-Pd₁@PDCN catalyzed aerobic oxidation of HMF. Reaction conditions: HMF 0.1 mmol, HMF/metal molar ratio=100:1, O₂ 10 mL min⁻¹, K₂CO₃ 0.4 mmol, water 2 mL, 90 °C.

4. Supplementary Tables

Table S1 Elemental analysis of different samples

Samples	N %	C %	H %
[CVIM]Cl	21.15	53.86	5.51
PECN	1.45	55.88	6.29
Au ₁ -Pd ₁ @PECN	1.42	54.42	5.29
PDECN	1.02	67.52	6.31
Au ₁ -Pd ₁ @PDECN	0.98	67.96	6.79
PDCN	1.62	90.09	8.01
Au ₁ -Pd ₁ @PDCN	1.53	89.73	7.51
PEGDMA	0	55.09	5.83
Au ₁ -Pd ₁ @PEGDMA	0	56.48	5.43

Table S2. Aerobic oxidation of HMF over different base amount^a

Entry	Mole of K ₂ CO ₃	HMF Conv. (%)	FDCA Yield (%)	FDCA Sel. (%)
1	0.1	81.5	61.7	75.6
2	0.2	92.4	72.5	78.4
3	0.3	99.9	80.3	80.3
4	0.4	99.9	99.0	99.0
5	0.5	99.9	96.2	96.8

^aReaction conditions: HMF 0.1 mmol, HMF/metal molar ratio=100:1, O₂ 10 mL min⁻¹, water 2 mL, 90 °C, 12 h.

Table S3 Aerobic oxidation of HMF over different control catalysts^a

Entry	Sample	Au/Pd ^b	Metal ^c (wt%)	Conv. ^d (%)	Yield (%)			Carbon balance (%)
					FFCA	HMFCA	FDCA	
1	Au ₁ -Pd _{0.2} @PECN	1:0.22	1.05	96.8	4.7	2.8	76.6	86.8
2	Au ₁ -Pd _{0.5} @PECN	1:0.49	1.22	93.5	1.3	0	83.8	91.0
3	Au ₁ -Pd _{1.3} @PECN	1:1.29	1.56	97.7	0	2.1	89.7	93.9

^a Reaction conditions: HMF 0.1 mmol, HMF/metal molar ratio=100:1, O₂ 10 mL min⁻¹, K₂CO₃ 0.4 mmol, water 2 mL, 90 °C, 12 h. ^b Au/Pd weight ratio. ^c Total metal loading. ^d The conversion of HMF.

Table S4 Comparison of supported catalysts in aerobic oxidation of HMF to FDCA

Entry	Catalyst	Pressure (bar)	HMF/ metal ^a	T (°C)	Yield ^b (%)	TON	Ref.
1	Pd/C@Fe ₃ O ₄	1	27.5	80	88.1(83.1)	24.2	[S1]
2	γ-Fe ₂ O ₃ @-HAP-Pd(0)	1	42.4	100	92.9(90.9)	39.4	[S2]
3	Au/HT	1	40	95	>99(89)	39.6	[S3]
4	C-Fe ₃ O ₄ -Pd	1	37	80	91.8(86.8)	34	[S4]
5	Pt-PVP-GLY	1	19.3	80	100(88)	19.3	[S5]
6	1.5Au ₃ Cu ₁ -Ti	10	100	95	>90(40)	>90	[S6]
7	1.5(AuCu)-Ti	10	100	95	99(97)	99	[S7]
8	Au ₈ -Pd ₂ /AC	3	200	60	99(90)	198	[S8]
9	Au-Pd/CNT	5	100	100	94(90)	94	[S9]
10	Pt/C-O-Mg	10	50	110	97(87)	48.5	[S10]
11	Ru/CTF-c	20	40	140	41.4(35.6)	16.6	[S11]
12	Ru(OH)x/MgO·La ₂ O ₃	2.5	20	140	98(96)	19.6	[S12]
13	Au/TiO ₂	20	100	30	71(66)	71	[S13]
14	Ru(4%)/MnCo ₂ O ₄	24(air)	33.6	120	99.1(-)	33.3	[S14]
			500	90	70.0(-)	350	
16	Au ₁ -Pd ₁ @PECN	1		100	90	99	This work
				200	90	81.3/81.6/80.3/ 81.0/80.2 ^c	162

^a Mole ratio of HMF to metal. ^b FDCA yield and recovered yield after several recycles in corresponding documents. ^c FDCA yield in the 1st, 2nd, 3rd, 4th and 5th run by controlling the reaction condition to give a moderate yield.

Additional explanation for Table S4 and activity comparison

Many heterogeneous catalysts have been developed for the oxidation of HMF to FDCA with O₂. Table S4 lists some typical efficient ones. Owing to the variation of reaction conditions, it is difficult to directly compare the activity of different catalytic systems. However, the yield, TON and stability of the catalyst are among the most important parameters to evaluate a catalytic system. Further, mild reaction conditions such as low temperature and atmospheric O₂ are preferable in the reaction. Because noble metals are high price and low natural abundant, therefore, design highly atom-efficient and stable noble metal based heterogeneous catalyst is highly desirable. As shown in Table S4, excessive noble metals were used in many cases, giving low TON and unsatisfied atom-efficiency of expensive noble metals. For example, TON of them were normally below 40 by using atmospheric O₂. Further, majority of previous heterogeneous

catalysts still suffered from deactivation during the recycling test. In this work, the constructed heterogeneous catalyst $\text{Au}_1\text{-Pd}_1@\text{PECN}$ afforded high yield of 99% and TON of 99% by using atmospheric O_2 . This activity here is superior to most of the previous ones and at least comparable to the best ones even under high O_2 pressure previously (Table S4). Increasing the HMF/metal molar ratio to 500 results in a moderate yield of 70% with a maximum TON of 350, which is the highest one so far. Compared to previous works, such high TON exceeds greatly (about 10 times) previous ones under atmospheric O_2 conditions (Table S4). This catalyst is stable and exhibits well reusability. Use of weak base K_2CO_3 also causes the reaction under a mild weak base condition to reduce the potential corrosion under strong basic condition. All of these suggest that our designed catalyst possesses high atom-efficiency of noble metals with stable activity under relatively mild conditions (low temperature, atmospheric O_2 and weak base environment). Additionally, mesoporous poly(ionic liquid)s (MPILs) supported noble metals nanoparticles are used as the heterogeneous catalyst in the conversion of HMF into FDCA for the first time and deliver high performance in this reaction. By contrast, previous studies mainly focused on the inorganic supports. The results of this work imply that MPILs combining the features of ILs, mesoporous materials and polymers are promising catalyst supports towards high performance heterogeneous catalysts, and therefore provide a promising new strategy to fabricate highly efficient catalytic systems for biomass conversion.

5. References

- S1 B. Liu, Y. S. Ren and Z. H. Zhang, *Green Chem.* 2015, **17**, 1610.
- S2 Z. H. Zhang, J. D. Zhen, B. Liu, K. L. Lv and K. J. Deng, *Green Chem.* 2015, **17**, 1308.
- S3 N. K. Gupta, S. Nishimura, A. Takagaki and K. Ebitani, *Green Chem.* 2011, **13**, 824.
- S4 N. Mei, B. Liu, J. D. Zheng, K. L. Lv, D. G. Tang and Z. H. Zhang, *Catal. Sci. Technol.* 2015, **5**, 3194.
- S5 S. Siankevich, G. Savoglidis, Z. F. Fei, G. Laurenczy, T. L. Alexander, N. Yan and P. J. Dyson, *J. Catal.* 2014, **315**, 67.
- S6 S. Albonetti, T. Pasini, A. Lolli, M. Blosi, M. Piccinini, N. Dimitratos, J. L. Sanchez, D. J. Morgan, A. F. Carley, G. J. Hutchings and F. Cavani, *Catal. Today* 2012, **195**, 120.
- S7 T. Pasini, M. Piccinini, M. Blosi, R. Bonelli, S. Albonetti, N. Dimitratos, J. A. Sanchez, M. Sankar, Q. He, C. J. Kiely, G. J. Hutchings and F. Cavani, *Green Chem.* 2011, **13**, 2091.
- S8 A. Villa, M. Schiavoni, S. Campisi, G. M. Veith and L. Prati, *ChemSusChem* 2013, **6**, 609.
- S9 X. Y. Wan, C. M. Zhou, J. S. Chen, W. P. Deng, Q. H. Zhang, Y. H. Yang and Y. Wang, *ACS Catal.* 2014, **4**, 2175.
- S10 X. W. Han, L. Geng, Y. Guo, R. Jia, X. H. Liu, Y. G. Zhang and Y. Q. Wang, *Green Chem.* 2016, **18**, 1597.
- S11 J. Artz and R. Palkovits, *ChemSusChem* 2015, **8**, 3832.
- S12 Y. Y. Gorbanev, S. Kegnæs, A. Riisager, *Top Catal.* 2011, **54**, 1318.
- S13 Y. Y. Gorbanev, S. K. Klitgaard, J. M. Woodley, C. H. Christensen and A. Riisager, *ChemSusChem* 2009, **2**, 672.
- S14 D. K. Mishra, H. J. Lee, J. Kim, H. S. Lee, J. K. Cho, Y. W. Suh, Y. J. Yid and Y. J. Kim, *Green Chem.* 2017, **19**, 1619.